Journal of The Electrochemical Society, **151** (11) A1954-A1960 (2004)
0013-4651/2004/151(11)/A1954/7/$7.00 © The Electrochemical Society, Inc.

Experimental Validation of a PEM Fuel Cell Model by Current Distribution Data

Hyunchul Ju and Chao-Yang Wang*,z

Electrochemical Engine Center and Department of Mechanical and Nuclear Engineering, The Pennsylvania State University, University Park, Pennsylvania 16802, USA

A three-dimensional, electrochemical-transport coupled model is applied to a 50 cm^2 proton exchange membrane (PEM) fuel cell and validated against the current distribution data experimentally measured earlier. A parallel computational methodology is employed to substantially reduce the computational time and make large-scale calculations involving millions of grid points possible. Simulation results are analyzed and validated against the available experimental data of current distribution under fully humidified conditions for two cathode stoichiometry ratios. The comparisons of simulations and experiments point out a lack of agreement in the current distribution, although the average polarization curves are matched nearly perfectly. The numerical simulations correctly capture the comma-shaped local polarization curves observed in the current distribution experiments.
 [DOI: 10.1149/1.1805523]

Manuscript submitted September 19, 2003; revised manuscript received June 11, 2004. Available electronically October 27, 2004.

Optimization of polymer electrolyte fuel cells (PEFC) requires a good understanding of the fuel cell fundamentals. Modeling and simulation have become important tools to aid our understanding of the complex and multidisciplinary PEFC system where electrochemical and transport processes are tightly coupled. A number of PEFC models of varying sophistication have been developed in the last decade.[1-10] These range from simplified one-dimensional models for individual components as well as whole cells to multiphysics, multidimensional, two-phase computational fuel cell dynamics (CFCD) modeling. While highly sophisticated CFCD simulations are capable of predicting many details, to date model validation has been limited to the cell overall polarization (or *I-V*) curve which is an integral outcome of many interacting phenomena.

It has been increasingly acknowledged that the global *I-V* curve is largely inadequate to validate comprehensive PEFC models. This inadequacy can perhaps best be illustrated by a numerical experiment shown in Fig. 1. In this experiment, a three-dimensional (3D) PEFC model (same as the one described in this work) is applied to a single-channel fuel cell using Gore-Select 18 μm membrane under the anode/cathode stoichiometry of 3/2, and anode/cathode inlet relative humidity of 42%/dry at the cell temperature of 80°C. Two cases are simulated using the same model for the cell voltage of 0.75 V. In case 1, the ionic resistance in two catalyst layers is included as is typically done in all of our fuel cell calculations, and the kinetic constant of oxygen reduction reaction (ORR) is estimated from the Pt loading. This case yields an average current density of 0.24 A/cm^2 at 0.75 V. In case 2 (hypothetical), however, we neglect the ionic resistance in two catalyst layers (which amounts to about twice that in the membrane) and then adjust the kinetic constant by 23% lower. By changing only two parameters (*i.e.*, catalyst layer resistance and kinetic constant of ORR), hypothetical case 2 produced exactly the same the average current density as in case 1, despite the fact that the two cases fundamentally differ in limiting mechanisms. Case 1 is dominated more by ohmic polarization, thereby exhibiting a slight increase in the local current density near the dry inlet as the membrane becomes more hydrated and falls only close to the outlet where oxygen depletion starts to take control. On the other hand, case 2 is dominated more by concentration polarization with little ohmic loss. As a result, the current distribution in case 2 closely follows the decline of oxygen concentration due to the stoichiometric effect (*i.e.*, 2).

Wang[12] concluded that it is the detailed validation against current and species distribution data that will permit an ultimate understanding of the electrochemical phenomena in PEFC as well as development of dependable computer-aided tools for design and product development. A main objective of the present paper is therefore to test a 3D PEFC model against the current distribution data most recently obtained by Mench *et al.*[13] for a 50 cm^2 cell. To apply the 3D model to such a real-scale fuel cell with a serpentine flow field, a large numerical mesh of the order of 1.3 millions grid points is needed, thus calling for an efficient parallel computational method. The remainder of this paper is organized as follows. We describe the 3D PEFC model in detail, including its physical governing equations as well as its numerical implementation in a commercial CFD package, STAR-CD parallel version. The Results and Discussion section summarizes the validation experiments and fully discusses simulation results in comparison with experimental data of the current distribution. Finally, major conclusions from this study along with areas for future work are presented.

Physical and Numerical Model

Model assumptions and description.—The 3D computational fuel cell dynamics (CFCD) model used in this paper is developed based on the work of Um *et al.*[6,9] The model is capable of predicting electrochemical and transport phenomena in all seven subregions of PEFCs: gas channels, diffusion and catalyst layers on both anode and cathode sides, and the ionomeric membrane.

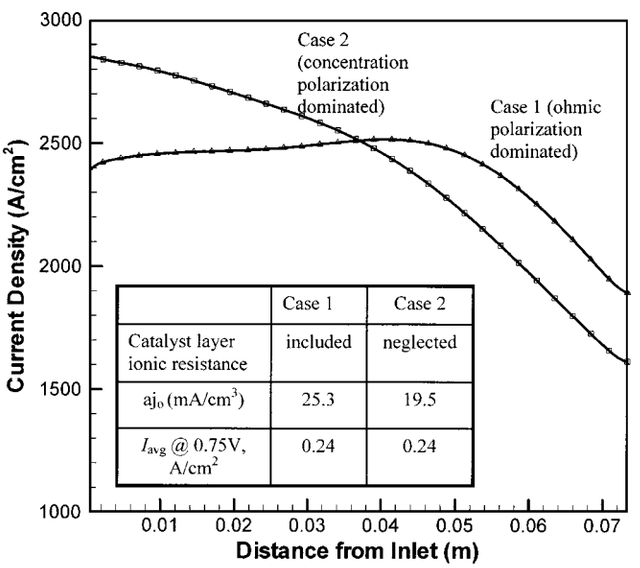

Figure 1. Local current density profiles along a single-channel fuel cell as predicted by the same computer model for two cases differing only in two model parameters.[11]

* Electrochemical Society Active Member.
z E-mail: cxw31@psu.edu

Table I. Single-phase steady-state PEFC model, governing equations with source terms.

	Conservation equations		Source terms
Mass	$\nabla \cdot (\rho \mathbf{u}) = 0$	[1]	
Momentum	$\frac{1}{\epsilon^2}\nabla \cdot (\rho \mathbf{u}\mathbf{u}) = -\nabla p + \nabla \cdot \tau + S_u$	[2]	In diffusion and catalyst layers: $S_u = -\frac{\mu}{K}\mathbf{u}$
Species	$\nabla \cdot (\mathbf{u}c_k) = \nabla \cdot (D_k^{eff}\nabla c_k) + S_k$	[3]	In catalyst layers: $S_k = -\frac{s_k j}{nF}$ For water in catalyst layers: $S_k = -\frac{s_k j}{nF} - \nabla\left(\frac{n_d}{F} I_e\right)$
Charge	$\nabla \cdot (\kappa^{eff}\nabla\phi_e) + S_\phi = 0$	[4]	In catalyst layers: $S_\phi = j$

Electrochemical reaction
$\Sigma_k s_k M_k^z = ne^-$ where M_k is the chemical formula of species k, s_k, the stoichiometry coefficient, and n, the number of electrons transferred.
HOR on anode $H_2 - 2H^+ = 2e^-$ [5]
ORR on cathode $2H_2O - O_2 - 4H^+ = 4e^-$ [6]

The following assumptions are made in the model: (*i*) ideal gas mixtures; (*ii*) isotropic and homogeneous electrode, catalyst layer, and membrane; (*iii*) incompressible and laminar flow due to small gas velocities; (*iv*) negligible ohmic potential drop due to very large electrical conductivity in the electronically conductive solid matrix of porous electrodes and catalyst layers, as well as in the current collectors; (*v*) single-phase assumption for water transport. Assumption *v* implies that water can exist in supersaturation in the gas phase, thus being similar to the treatment of Springer *et al.*[1] where the water activity is allowed to be greater than unity. However, there exists significant flooding in the cathode of a PEFC operating under fully humidified feed and high current densities. Excessive liquid water will prevent oxygen transport to the reaction sites by clogging the pores of the gas diffusion layer (GDL). As a result, the effective porosity of the GDL for gas transport may be significantly lower than its intrinsic porosity in the severe flooding situation.[4] In the present work, this effective porosity is used as an adjustable parameter to account for the flooding effects. Also, passivation of catalyst sites by the presence of liquid water in the catalyst layer is not considered.

Under these assumptions, the PEFC model consists of the conservation equations of mass, momentum, chemical species, and charge. A single-domain approach is used to make a single set of governing equations valid for all subregions. Thus no interfacial conditions are required to be specified at internal boundaries between various regions. Table I lists all these governing equations and their respective source terms representing various volumetric sources/sinks in subregions of a fuel cell. It should be noticed that superficial velocities are used for the porous regions in order to automatically ensure mass flux continuity at the interface between porous and nonporous regions. Also notice that intrinsic transport properties in the porous regions are modified into effective properties to account for the effects of porosity and tortuosity in the porous region using the Bruggeman correlation.[14] The source terms in the momentum equations are devised to recover Darcy's law under the limiting condition where the permeability of the porous medium is

Table II. Physical parameters and properties.

Description	Value
Anode/cathode gas diffusion layers thickness	0.300 mm
Anode/cathode catalyst layers thickness	0.010 mm
Membrane thickness (Nafion 112)	0.051 mm
Effective porosity of anode/cathode gas diffusion layers, ϵ_{GDL}^{eff}	0.17
Effective porosity of anode/cathode catalyst layers, ϵ_{cat}^{eff}	0.17
Volume fraction of ionomer in anode/cathode catalyst layers, ϵ_{mc}	0.2
Permeability of anode/cathode gas diffusion layers, K	1.12×10^{-14} m^2
Exchange current density × specific surface area on anode, $aj_{0,a}^{ref}$	1.0×10^9 A/m^3
Exchange current density × specific surface area on cathode, $aj_{0,c}^{ref}$	2.5×10^3 A/m^3
H_2 reference molar concentration, $c_{H_2,ref}$	40.88 mol/m^3
O_2 reference molar concentration, $c_{O_2,ref}$	40.88 mol/m^3
Anodic and cathodic transfer coefficients for HOR	$\alpha_a = \alpha_c = 1$
Cathodic transfer coefficient for ORR	$\alpha_c = 1$
Dry membrane density, $\rho_{dry,mem}$	1980 kg/m^3
Equivalent weight of membrane, EW	1.1 kg/mol
Faraday constant, F	96,487 C/mol
Universal gas constant, R	8.314 J/mol K
H_2 diffusivity in membrane, $D_{H_2}^{mem}$	2.59×10^{-10} m^2/s
O_2 diffusivity in membrane, $D_{O_2}^{mem}$	1.22×10^{-10} m^2/s
H_2 diffusivity in the anode gas channel, $D_{0,H_2,a}$	1.1028×10^{-4} m^2/s
H_2O diffusivity in the anode gas channel, $D_{0,H_2O,a}$	1.1028×10^{-4} m^2/s
O_2 diffusivity in the cathode gas channel, $D_{0,O_2,c}$	3.2348×10^{-5} m^2/s
H_2O diffusivity in the cathode gas channel, $D_{0,H_2O,c}$	7.35×10^{-5} m^2/s

low and hence the velocity is small. The source term in the charge equation is used to describe the transfer current between the solid matrix and the electrolyte phase inside each of the anode and cathode catalyst layers. The transfer current densities are expressed as follows

$$\text{Anode } j = aj_{0,a}^{\text{ref}}\left(\frac{c_{H_2}}{c_{H_{2,\text{ref}}}}\right)^{1/2}\left(\frac{\alpha_a + \alpha_c}{RT}F\eta\right) \quad [7]$$

$$\text{Cathode } j = -aj_{0,c}^{\text{ref}}\left(\frac{c_{O_2}}{c_{O_{2,\text{ref}}}}\right)\exp\left(-\frac{\alpha_c}{RT}F\eta\right) \quad [8]$$

These kinetic expressions represent the hydrogen oxidation reaction (HOR) in the anode catalyst layer and ORR in the cathode catalyst layer, respectively. These are modified from the general Butler-Volmer equation. The HOR kinetic expression is derived by linearizing the Butler-Volmer equation on the assumption that the HOR reaction is facile and hence the surface overpotential is small. On the other hand, the ORR kinetic reaction is slow, causing high overpotential. Therefore the ORR kinetic expression is obtained by neglecting the anodic reaction term of the Butler-Volmer equation. It should be noted that the ORR is assumed to be a first-order reaction based on the early experimental work of Bernardi and Verbrugge[2] and Gottesfeld and Zawodzinski.[15] By assuming the reference open-circuit potentials of anode and cathode to be zero and a function of temperature, respectively, the expressions of surface overpotential for anode and cathode sides can be defined, respectively, as

$$\text{Anode side } \eta = -\phi_e \quad [9]$$

$$\text{Cathode side } \eta = V_{\text{cell}} - \phi_e - U_{\text{oc}} \quad [10]$$

where U_{oc} is given by[16]

$$U_{\text{oc}} = 1.23 - 0.9 \times 10^{-3}(T - 298) \quad [11]$$

The source terms in the species equations represent production or consumption of species k due to the two electrochemical reactions (*i.e.*, HOR and ORR) and the electro-osmotic drag of water from the anode to the cathode.

The mass diffusion coefficient of species k, D_k, in the anode and cathode gas channels is calculated as a function of temperature and pressure.[17] For the porous regions of a PEM fuel cell, such as the gas diffusion and catalyst layers, the expression is modified into the effective species diffusivity, D_k^{eff} using Bruggman correlation[14]

$$D_k = D_{0,k}\left(\frac{T}{T_0}\right)^{3/2}\left(\frac{P_0}{P}\right) \quad \text{for gas channels} \quad [12]$$

$$D_k^{\text{eff}} = \epsilon_i^{1.5}D_k \quad \text{for porous regions} \quad [13]$$

Species k may also be dissolved in the membrane phase and thus has a diffusivity corresponding to the dissolved species, which is usually a few orders of magnitude lower than that in gas (see Table II for hydrogen and oxygen diffusion coefficients in the membrane phase). The water diffusivity, D_w^{mem}, the proton conductivity, σ_{mem} in the membrane, and the electro-osmotic drag coefficient for water, n_d, are all functions of the water content of the membrane, λ, which was expressed as a function of the water activity, a, by Springer *et al.*[1] as follows

$$a = \frac{C_w^g RT}{P^{\text{sat}}} \quad [14]$$

$$\lambda = \begin{cases} 0.043 + 17.81a - 39.85a^2 + 36.0a^3 & \text{for } 0 < a \leq 1 \\ 14 + 1.4(a - 1) & \text{for } 1 < a \leq 3 \end{cases} \quad [15]$$

Equation 15 expresses equilibrium water uptake of the membrane. We note, however, a more recent study of Berg *et al.*[18] that proposed a nonequilibrium theory of water transport across the membrane-gas-phase interface. While this is an interesting hypothesis, much work is needed to fully understand the fundamental implications of this nonequilibrium theory as well as to ascertain its applicability in various fuel cell conditions. Thus, the present model still employs the equilibrium membrane relation given by Eq. 15, so as to be consistent with all prior models (*e.g.*, Ref. 1-8).

The proton conductivity in the membrane and the electro-osmotic drag coefficient of water implemented in the present model follow the empirical correlations of Springer *et al.*[1]

$$\kappa_{\text{mem}} = (0.5139\lambda - 0.326)\exp\left[1268\left(\frac{1}{303} - \frac{1}{T}\right)\right] \quad [16]$$

$$n_d = \frac{2.5\lambda}{22} \quad [17]$$

Again using the Bruggman correlation, the proton conductivity of the anode and cathode catalyst layers is given by

$$\kappa^{\text{eff}} = \epsilon_{mc}^{1.5}\kappa_{\text{mem}} \quad [18]$$

where ϵ_{mc} is the volume fraction of ionomer in the anode or cathode catalyst layer.

The equivalent water concentration in the membrane is defined as

$$c_w^{\text{mem}} = \frac{\rho_{\text{dry,mem}}\lambda}{EW} \quad [19]$$

The water diffusivity in Nafion membranes follows that of Motupally *et al.*[19]

$$D_w^{\text{mem}} = \begin{cases} 3.1 \cdot 10^{-7}\lambda(e^{0.28\lambda} - 1) \cdot e^{(-2346/T)} & \text{for } 0 < \lambda \leq 3 \\ 4.17 \cdot 10^{-8}\lambda(1 + 161e^{-\lambda}) \cdot e^{(-2346/T)} & \text{otherwise} \end{cases} \quad [20]$$

Once the electrolyte phase potential, ϕ_e, and the proton conductivity of the membrane, σ_{mem}, are obtained, the local current density, I, can be calculated by

$$I = -\kappa_{\text{mem}}\nabla\phi_e \quad [21]$$

The average current density can be obtained by taking the surface average of local current density over the entire membrane

$$I_{\text{avg}} = \frac{1}{A_{\text{mem}}}\int_{A_{\text{mem}}} IdA \quad [22]$$

Boundary conditions.—Equation 1 through 4 in Table I form a complete set of governing equations for six unknowns: **u**, p, c_{H_2}, c_{O_2}, c_{H_2O}, and ϕ_e. By use of the single-domain approach, boundary conditions are required only at the external surfaces of the computational domain. The no-flux condition is applied to the external surfaces except for the inlets and outlets of the anode/cathode gas channels. At the anode/cathode inlet, the inlet species concentrations, $c_{k,\text{in}}$, are determined by the inlet pressure and humidity conditions, namely, $c_k = p_k/RT$. Herein, the partial pressure of water vapor at the inlet is equal to the saturation pressure at the prescribed humidification temperature. The anode/cathode inlet velocities can be calculated by their respective stoichiometric flow ratios, ζ_a and ζ_c, defined as the ratio of the amount of reactant supplied to the amount of reactant required by the electrochemical reaction to generate a specified reference current density, I_{ref}

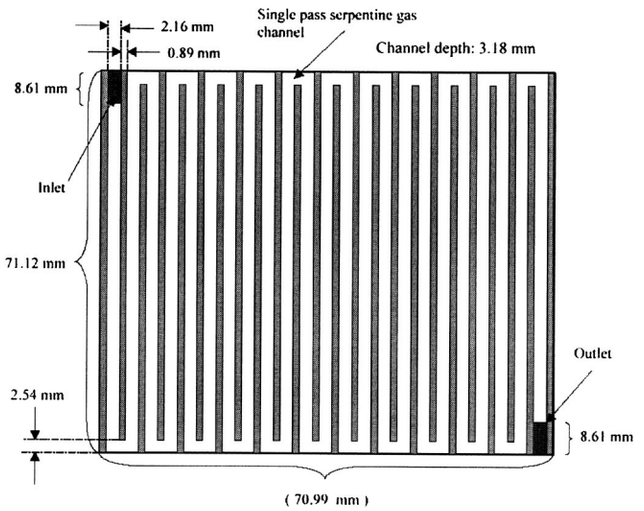

Figure 2. Schematic diagram of the 50 cm^2 instrumented test cell with relevant dimensions of flow field.

$$V_{a,in} = \zeta_a \frac{I_{ref}}{2FC_{H_2,in}} \frac{A_{react}}{A_{a,in}} \quad [23]$$

$$V_{c,in} = \zeta_c \frac{I_{ref}}{4FC_{O_2,in}} \frac{A_{react}}{A_{c,in}} \quad [24]$$

The outlet species and velocity conditions are the fully developed ones, *i.e.*, the gradient of each variable is zero.

STAR-CD implementation.—The PEFC model described above is implemented into a commercial computational fluid dynamics (CFD) package, STAR-CD, basing on its user-coding capability.[20] All source terms of conservation equations of momentum, chemical species, and charge are specified in the user code.

To carry out the detailed validation study against the current distribution data of Mench *et al.*,[13] a numerical mesh for the PEFC model is created for the experimental cell. Figure 2 and 3 show the 2D and 3D schematic diagrams of the 50 cm^2 instrumented test cell with a single-path serpentine flow field. Orthogonal but nonuniform grid is used in various subregions. Based on the grid-independence study by Meng and Wang,[21] roughly 1.3 million computational cells are applied to this fuel cell geometry.

Parallel computing and performance.—In this work, the parallel computing technique is used in order to facilitate these large-scale simulations. Several domain decomposition options were investigated by Meng and Wang[21] in an attempt to maximize the parallel efficiency and minimize the communication overhead between processors. Using the optimized option, the computational mesh, user codes, and data files of the PEFC model are massively parallelized. All simulations for the validation study are carried out on an in-house Linux PC cluster, where 50 processors of 1.4 GHz AMD Athelon Thunderbird CPU and 512MB DDR SDRAM are connected together by a local 100 Mbps switched Ethernet network. The high parallel efficiency was reported in Meng and Wang,[21] where more than a seven time speed-up was achieved, when 10 CPUs are used. Using 10 CPUs, the current PEFC model with 1.3 million computational cells roughly requires 24 s per iteration. On the other hand, when a single high-speed PC (2 GHz) is used, about 130 s was estimated per iteration. Usually 300-400 iterations are needed to complete a typical case. So one simulation takes roughly 2-3 h on the 10 parallel machines and 10-15 h on the single high-end PC.

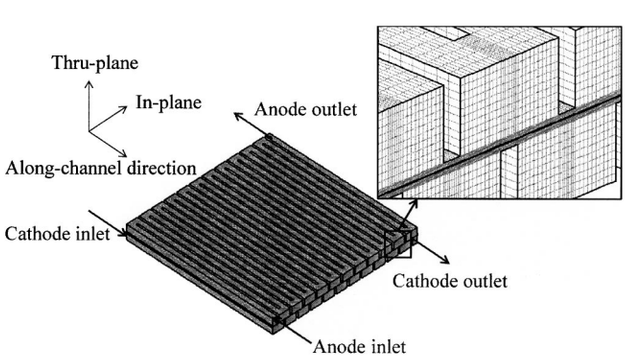

Figure 3. Mesh configuration for the PEFC numerical model.

Results and Discussion

Validation experiments.—The current distribution data used in the present study were made available most recently by Mench *et al.*[13] The experiments were performed in a segmented cell of 50 cm^2 using a multichannel potentiostat. The membrane electrode assembly (MEA), made of a Nafion 112 membrane, was not segmented, in accordance with the model assumptions made earlier herein. The cell's flow field, a single-pass serpentine, is given in Fig. 2 along with relevant dimensions.

Current density distribution measurements were made under the conditions of 80°C cell temperature and 1.5 atm inlet pressure on both anode and cathode. The humidification temperatures were 90 and 80°C for the anode and cathode, respectively. The anode stoichiometry was set to be 2.5 at 0.75 A/cm^2, high enough to minimize the anode concentration polarization effect. The cathode stoichiometry was varied systematically to investigate the oxygen concentration polarization, a dominant phenomenon in fully-humidified PEM fuel cells. It should be emphasized that the stoichiometry used in this experimental work is based on the reference current density of 0.75 A/cm^2; as such, the anode and cathode flow rates were constant under all current densities. Other details of the experiments can be found in Mench *et al.*[13]

Model validation.—In the present model validation, both cathode stoichiometry cases of 2.0 and 3.0 in the experimental work of Mench *et al.*[13] are utilized, representing a practical reasonable stoichiometry and a high cathode stoichiometry, respectively. As expected and to be shown shortly, the local current density in the lower stoichiometry case is less uniform than the high stoichiometry case.

Several issues pertinent to numerical simulations of the two experiments are worth noting. First, a contact resistance of 130 $m\Omega$ cm^2 is applied in the model to account for all interfacial resistances within the instrumented fuel cell, *e.g.*, at the loose interface between the catalyst coated membrane (CCM) and the GDL and the contact between GDL and the current collector land. This total contact resistance value is slightly larger than that in state-of-the-art single cells, due largely to the nature of the segmented cell having many more mating interfaces rather than two continuous surfaces. Second, as both experiments were carried out under fully-humidified anode/cathode conditions, severe flooding of the electrode is expected; as such, following Springer *et al.*,[4] the effective porosity of GDL, ϵ_{GDL}^{eff}, available for gas transport is adjusted to be 0.17 to approximate the flooding effect by liquid water. Finally, the effect of GDL compression is considered in a way that the in-plane permeability of the portion of the GDL above the landing area is drastically reduced, resulting in virtually no flow (or bypass) of gas through the GDL above each landing. Other parameters used in the simulations are listed in Table II, including the relevant dimensions and properties of the MEA.

Figure 4 compares the simulated average polarization curve with the experimental data for the case of lower cathode stoichiometry. Good agreement is seen in the global performance. For the same case, the local polarization curves from both simulation and experi-

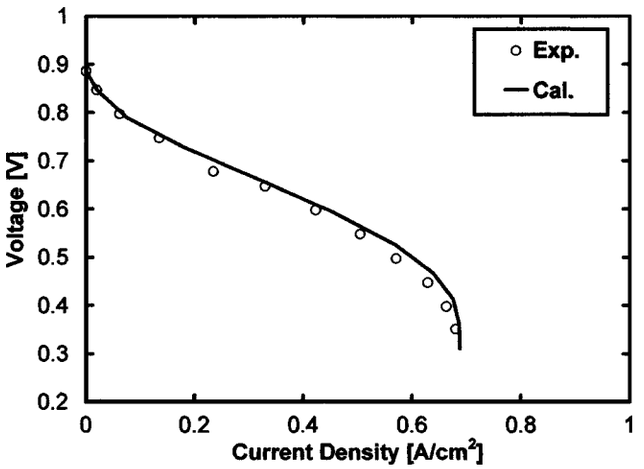

Figure 4. Measured and calculated average polarization curves for cathode stoichiometry of 2.0 at 0.75 A/cm^2.

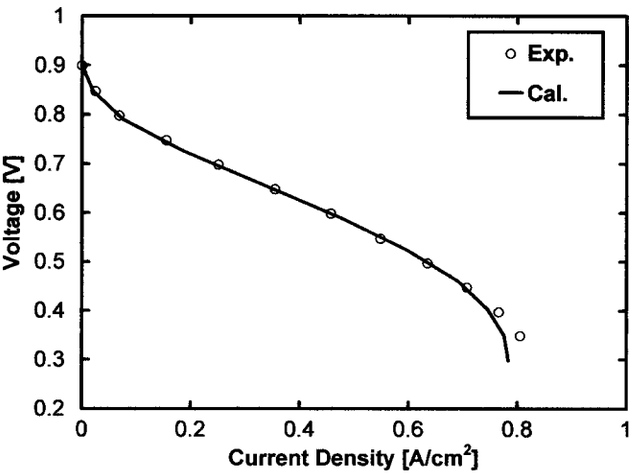

Figure 6. Measured and calculated average polarization curves from for cathode stoichiometry of 3.0 at 0.75 A/cm^2.

ment are presented in Fig. 5 with respect to the fractional location along the cathode flow path. It is clearly shown that there is an inadequate agreement between the two sets of localized *I-V* curves, especially in comparison with Fig. 4. Nonetheless, experimentally observed severe mass-transport limitations, exhibited as the comma-shaped curves in Fig. 5 in the outlet region ($x/L = 0.804$ and 0.891) and at low cell voltages, are correctly captured by the present model, although the model underestimates the mass-transport limitation. The severe mass-transport limitation is attributed to hindered oxygen transport through GDL pores partially filled with liquid water and hence causing reduced GDL porosity for gas diffusion. At lower cell voltages, the local current density in the upstream becomes higher, thus leading to more oxygen depletion and hence less current output downstream.

Figure 6 displays a comparison of the simulated and measured average polarization curves for the case of high cathode stoichiometry, and Fig. 7 shows the local polarization curves for the same case. Once again, similar to the case of low cathode stoichiometry, it is seen that the model validation against the average polarization curve is excellent, but the agreement in the local polarization curves is much less satisfactory. In Fig. 7, the predicted local polarization curves do not exhibit severe oxygen transport limitation, and they stay closely together, all indicative of the reduced mass-transport limitation thanks to the higher gas flow rate in the cathode. Comparing Fig. 6 directly with Fig. 4 clearly shows that the bulk fuel cell performance is improved at the high cathode stoichiometry.

Figures 8 and 9 plot the current distributions with the dimensionless distance along the cathode flow path for the low and high cathode stoichiometry cases, respectively. Both simulated and measured current distributions are shown for cell voltages ranging from 0.85 to 0.35 V. At high cell voltages (from 0.85 through 0.65 V in Fig. 8 and 9) or low average current densities, a nearly homogeneous distribution results in both simulations and experiments, indicating the absence of oxygen transport limitation throughout the cell. At low cell voltages (from 0.55 through 0.35 V in Fig. 8 and 9), however, the local current density in both simulations and experiments declines along the flow direction in general, demonstrating that oxygen depletion takes place. In addition, it is seen that the simulated current densities near the cathode inlet consistently overpredict the experimental data. This could be due to the fact that the experimental cell was not isothermal due to cell internal heating, which leads to a slightly higher temperature in the membrane. As a result, while fully humidified at 80°C, the inlet gas is less than 100% humidified relative to the higher membrane temperature, leading to a higher mem-

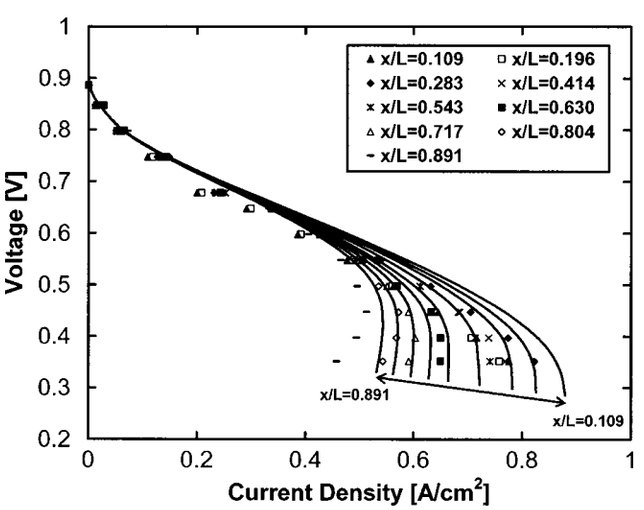

Figure 5. Comparison of local polarization curves simulated (lines) and measured (symbols) for cathode stoichiometry of 2.0 at 0.75 A/cm^2.

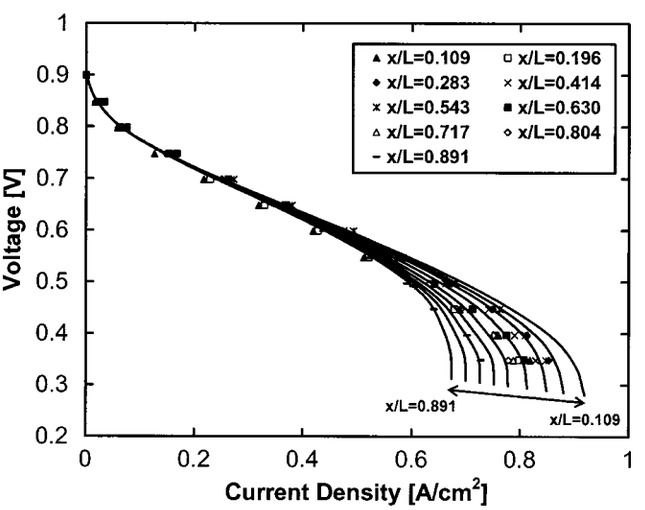

Figure 7. Comparison of local polarization curves simulated (lines) and measured (symbols) for cathode stoichiometry of 3.0 at 0.75 A/cm^2.

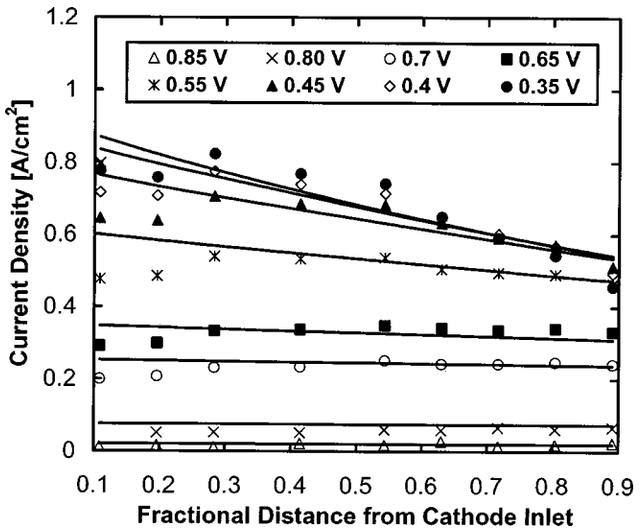

Figure 8. Comparison of simulated (lines) and measured (symbols) current distributions for cathode stoichiometry of 2.0 at 0.75 A/cm^2.

brane resistance and hence lower performance in the inlet region. In the middle of the cell, electrochemically produced water begins to make the cathode gas 100% humidified even relative to the higher membrane temperature and, thus, the highest current density results. Such a phenomenon can only be addressed by a nonisothermal PEFC model, which will be reported in a separate publication.

Figure 10 illustrates the simulated current density contours over the membrane at the cell voltage of 0.31 V and the cathode stoichiometry of 2.0, while Fig. 11 displays the contours for 0.29 V and cathode stoichiometry of 3.0. These results, while unattainable from experimentation, show a wealth of current nonuniformity features over the entire cell of 50 cm^2. First, the downstream effect of oxygen at low stoichiometry dominates the overall current distribution. Second, the current density in areas covered by gas channels is distinctively lower than that covered by lands. Thus, there exists a strong rib effect, particularly after GDL is compressed. Finally, high current density zones are found in the U-turn regions where the oxygen concentration at the catalyst surface is higher due to the

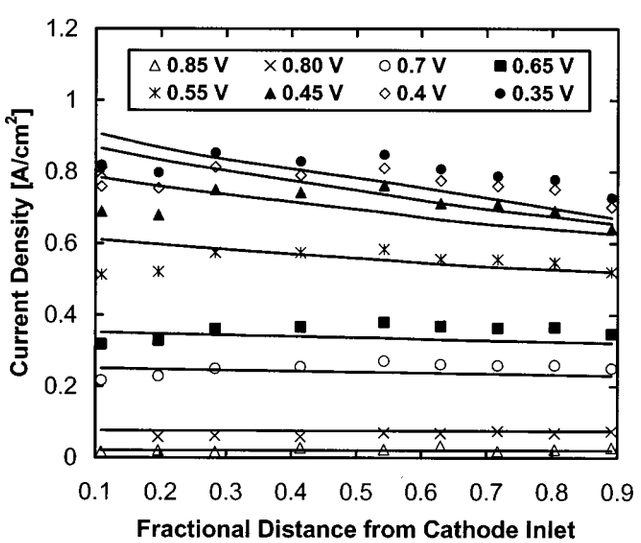

Figure 9. Comparison of simulated and measured current distributions for cathode stoichiometry of 3.0 at 0.75 A/cm^2.

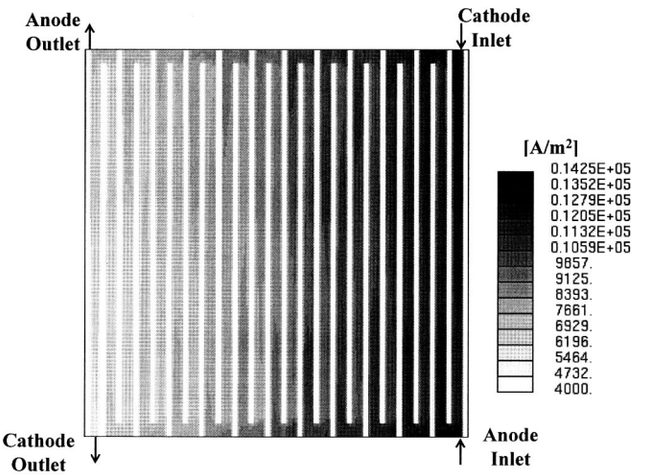

Figure 10. Current density contours in the middle of the membrane for cathode stoichiometry of 2.0 at $V_{cell} = 0.31$ V and $I_{avg} = 6874$ A/m^2.

mixing effect induced by gas vortical flow in each U-turn. Studying these phenomena by the simulation tool provides a major benefit for fuel cell engineering.

Conclusions

A three-dimensional, single-phase, isothermal PEFC model has been applied to a 50 cm^2 fuel cell operated with fully humidified gas feed and validated against the current distribution data measured earlier. Major conclusions can be summarized as follows:

It is clearly demonstrated that experimental validation of multiphysics PEFC models must be done against data at the distribution level. Validation against global *I-V* curves is insufficient and often misleading.

Parallel computing using inexpensive PC clusters can substantially cut down the computational time and make it possible to run large-scale simulation for PEFC involving millions of grid points on a routine basis. The parallel computational efficiency is found to be greater than 70% for fuel cell simulations. The CPU time for each simulation takes approximately 2 h for 1.3 million computational cells using 10 CPUs.

There is excellent agreement in the global polarization curve between the simulations and experiments for both cases of cathode

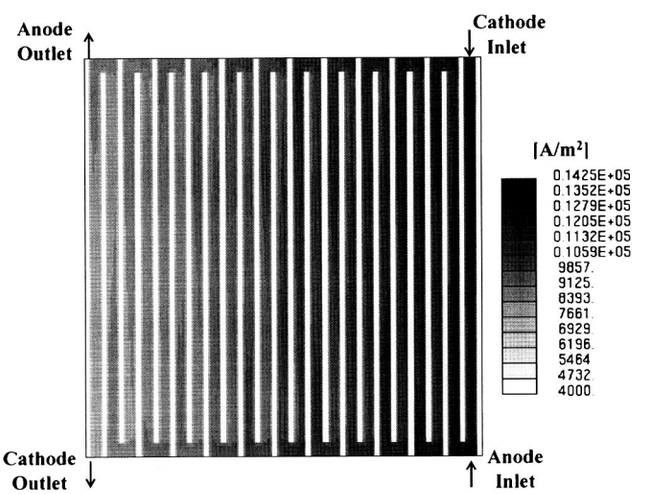

Figure 11. Current density contours in the middle of the membrane for cathode stoichiometry of 3.0 at $V_{cell} = 0.29$ V and $I_{avg} = 7834$ A/m^2.

stoichiometry, but the agreement on the current distribution level is not yet satisfactory, and more remains to be done in order to reconcile the discrepancies seen at the distribution level.

The numerical simulations nicely reproduced a key feature of the current distribution experiments, *i.e.*, the comma-shaped local *I-V* curves near the cathode outlet and at low cell voltages.

More recent research has indicated a need to validate comprehensive CFCD models against distribution data of multiple parameters, such as current and species distributions. This possibility is becoming a reality as the new experimental technique to measure current and species (*e.g.*, water) distributions simultaneously has emerged.[22,23] Efforts are continuing to validate CFCD models against multiple arrays of distribution data in order to develop a full understanding of PEFC fundamentals.

Acknowledgments

This research is funded by ConocoPhillips and DOE under the DOE cooperative agreement no. DE-FC26—01NT41098. Thanks are also due to Dr. S. Um for providing the fuel cell model, to Dr. H. Meng for providing a parallelized STAR-CD user code, and to Dr. Matthew Mench for useful discussions on the experimental data.

The Pennsylvania State University assisted in meeting the publication costs of this article.

List of Symbols

a	water activity
A	area, m^2
c	molar concentration, mol/m^3
D	mass diffusivity of species, m^2/s
EW	equivalent molecular weight of membrane, kg/mol
F	Faraday constant, 96,487 C/mol
I	current density, A/m^2
j	transfer current, A/m^3
K	hydraulic permeability, m^2
n	number of electrons transferred in electrochemical reaction
n_d	electro-osmotic drag coefficient
p	pressure, Pa
R	the universal gas constant, 8.314 J/mol K
s	stoichiometry coefficient in electrochemical reaction
S	source term in transport equation
T	temperature, K
$\mathbf{u}$	velocity vector, m/s
V_{cell}	cell potential, V
U_{oc}	open-circuit potential, U_{oc}

Greek

α	transfer coefficient
ϵ	volume fraction of gas phase in porous region
ϵ_{mc}	volume fraction of ionomer in catalyst layer
ζ	stoichiometry flow ratio
η	overpotential, V
κ	ionic conductivity, S/m
λ	membrane water content, mol H_2O/mol SO_3^-
μ	fluid viscosity, kg/m s
ρ	density, kg/m^3
σ	ionic conductivity, S/m
τ	viscous stress, N/m^2
ϕ	phase potential, V

Superscripts

eff	effective value in porous region
g	gas
mem	membrane
ref	reference
sat	saturation

Subscripts

a	anode
avg	average
c	cathode
cat	catalyst
e	electrolyte
GDL	gas diffusion layer
H_2	hydrogen
i	regions index
in	channel inlet
k	species index
mem	membrane
O_2	oxygen
react	electrochemical reaction
ref	reference
sat	saturation
u	momentum equation
w	water
Φ	potential equation
0	standard condition, 298.15 K and 101.3 kPa (1 atm)

References

1. T. E. Springer, T. A. Zawodinski, and S. Gottesfeld, *J. Electrochem. Soc.*, **136**, 2334 (1991).
2. D. M. Bernardi and M. W. Verbrugge, *AIChE J.*, **37**, 1151 (1991).
3. D. M. Bernardi and M. W. Verbrugge, *J. Electrochem. Soc.*, **139**, 2477 (1992).
4. T. E. Springer, M. S. Wilson, and S. Gottesfeld, *J. Electrochem. Soc.*, **140**, 3513 (1993).
5. V. Gurau, H. Liu, and S. Kakac, *AIChE J.*, **44**, 2410 (1998).
6. S. Um, C. Y. Wang, and K. S. Chen, *J. Electrochem. Soc.*, **147**, 4485 (2000).
7. S. Dutta, S. Shimpalee, and J. W. Van Zee, *J. Appl. Electrochem.*, **30**, 135 (2000).
8. D. Natarajan and T. V. Nguyen, *J. Electrochem. Soc.*, **148**, A1324 (2001).
9. S. Um and C. Y. Wang, *J. Power Sources*, **125**, 40 (2004).
10. H. Meng and C. Y. Wang, *J. Electrochem. Soc.*, **151**, A358 (2004).
11. Y. Wang, Private communications, Jan 2003.
12. C. Y. Wang, in *Handbook of Fuel Cells*, Vol. 3, W. Vielstich, A. Lamm, and H. Gasteiger, Editors, pp. 337-348, Wiley and Sons Ltd., London (2003).
13. M. M. Mench, C. Y. Wang, and M. Ishikawa, *J. Electrochem. Soc.*, **150**, A1052 (2003).
14. R. E. Meredith and C. W. Tobias, in *Advances in Electrochemistry and Electrochemical Engineering 2*, C. W. Tobias, Editor, Interscience Publishers, New York (1962).
15. S. Gottesfeld and T. A. Zawodzinski, in *Advances in Electrochemical Science and Engineering*, Vol. 5, C. Tobias, Editor, p. 195, John Wiley & Sons, New York (1997).
16. C. Berger, *Handbook of Fuel Cell Technology*, Prentice-Hall, New York (1968).
17. R. B. Bird, W. E. Stewart, and E. N. Lightfood, *Transport Phenamena*, John Wiley & Sons, New York (1960).
18. P. Berg, K. Promislow, J. St. Pierre, J. Stumper, and B. Wetton, *J. Electrochem. Soc.*, **151**, A341 (2004).
19. S. Motupally, A. J. Becker, and J. W. Weidner, *J. Electrochem. Soc.*, **147**, 3171 (2000).
20. STAR-CD Version 3.15 methodology, CD-Adapco Group (2001).
21. H. Meng and C. Y. Wang, *Chem. Eng. Sci.*, **59**, 3331 (2004).
22. M. M. Mench, Q. L. Dong, and C. Y. Wang, *J. Power Sources*, **124**, 90 (2003).
23. X. G. Yang, N. Burke, C. Y. Wang, K. Tajiri, and K. Shinohara, *J. Electrochem. Soc.*, In press.